CHAPTER 1
LASER SYSTEMS AS REMOTE SENSORS AND THE UPC LIDAR

Laser remote sensing of atmospheric properties from a single location is referred to as *LIDAR,* an acronym for ***LI**ght **D**etection **A**nd **R**anging*.

Lidar systems are used to monitor pollution of the air nearby cities and industrial plants. At airports, wind direction and speed can be measured with lidar systems and to provide early-warning signals in case of wind shear effects [133]. Airborne lidars are used to analyse the chemical composition of the stratosphere and others.

Lidar applications for remote sensing of the atmosphere continue to expand as new optical technologies become available. Thus, future lidar systems will be suitable for ground-based, airborne, and shipborne deployment. Lidar systems also measure ozone concentrations in the lower troposphere; small-scale turbulence effects on the exchange of chemical species and energy between the free atmosphere and land; the sea surfaces; and cloud and aerosol structure. Such instruments promise to have a lasting impact on atmospheric research and climate monitoring.

This chapter provides an up-to-date review of the laser probing techniques technologically available and a general overview of lidar system developed at the Polytechnic University of Catalonia (UPC).

1. REMOTE SENSING USING OPTICAL RADARS

Lidar systems are the counterpart of conventional radars except that microwave radiation is replaced by laser radiation [5][19].

In lidar, the emission of a short laser pulse is followed by the reception of a portion of the radiation reflected from a distant target or from atmospheric constituents such as molecules, aerosols, clouds, or dust (Fig.1). The incident laser radiation interacts with these constituents, causing alterations in the intensity and/or wavelength according to the strength of this optical interaction and the concentration of the interacting species in the atmosphere. Consequently, some information on the composition and physical state of the atmosphere can be deduced from the lidar data. In addition, the range to the interacting species can be determined from the temporal delay of the backscattered radiation [113][47][81].

Under optimal conditions, lidars can be extremely sensitive. An example is the detection of sodium and lithium atoms in the stratosphere at ranges greater than *90 km* and in concentrations, as low as a few atoms per cubic centimeter. More commonly, detection ranges are on the order of a few hundred meters to several kilometers and concentration levels on the order of parts per million to parts per billion.

The use of optical backscatter to measure properties of the atmosphere is not new in the field of optical radars. Large *searchlights* [26] pioneered optical radars in the early 1900's. This field was greatly advanced by the laser, which offers narrow spectral width *(less than 0.01 nm),* a frequency or color which is often tunable of switchable by means of non-linear crystals and high peak power *(> 1 MW)* available in short pulses *(1 μs)* and in a narrow beam.

Early lidar measurements were made in 1962 by Fiocco and Smullin [202] who bounced a laser beam off the moon and also investigated the turbid layers in the upper atmosphere, and in 1963 by Ligda [189], who used a ruby laser to obtain the first lidar measurements of cloud heights and tropospheric aerosols.

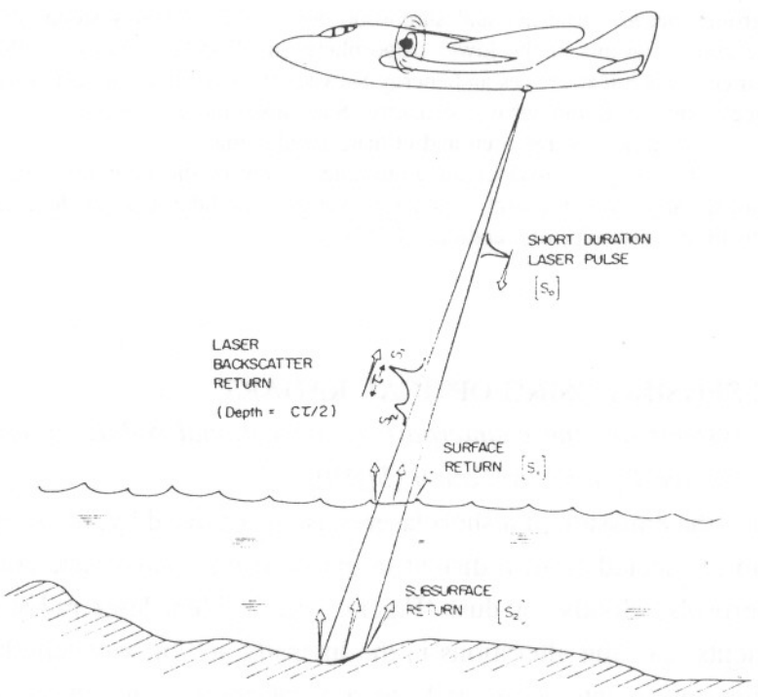

Fig.1 Pictorial representation of an airborne lidar [25].

2. OPTICAL REQUIREMENTS FOR LASER RADARS

2.1 Atmospheric transmission windows

For a laser beam to detect a species at a long distance, the beam must not be appreciably attenuated by the intervening atmosphere. *The output wavelength of the laser must therefore lie in a spectral transmission window of the atmosphere.* This will be discussed in more detail in Chap.2. However, the most useful transparent spectral ranges are the visible *(0.4 to 0.7 μm),* near-infrared *(0.7 to 1.5 μm),* and *3-* to *5-μm* and *9-* to *13-μm* regions [79][105].

2.2 Optical interaction of lasers with atmospheric species

The primary influence of the atmosphere on a low-power laser beam is through scattering and absorption. Both processes cause an attenuation of the beam according to *Bouguer's or Beer's law*

$$I = I_0 e^{-\alpha R} \tag{1}$$

where I is the intensity of the optical beam after transmission over a distance R, α is the atmospheric extinction coefficient, and I_0 is the initial intensity of the beam. It is possible the express α as a sum of terms

$$\alpha = \alpha_{Ray} + \alpha_{Mie} + \alpha_{Raman} + \alpha_{abs} \tag{2}$$

where α_{Ray}, α_{Mie} and α_{Raman} are the extinction coefficients related to Rayleigh, Mie and Raman scattering, respectively, and α_{abs} is the molecular absorption coefficient [79].

Rayleigh scattering is due to particles in the atmosphere, such as molecules or fine dust, that are much smaller than the optical wavelength, λ, of the laser. *Mie scattering* is associated with larger particles such as aerosols whose size is on the order of λ. Rayleigh and Mie processes are elastic scattering, i.e. the scattered light is the same wavelength (color) as the incident laser beam. *Raman scattering* is an inelastic interaction of the optical beam involving excitation of the energy levels of a molecule and reradiation at a different wavelength. *Absorption* of the laser beam is a resonant interaction (direct absorption) leading to excitation of the molecule, followed possibly by *fluorescence* [25][9]

The range of cross-sections observed for each process is schematically presented in Tab.1 [25]. Differential absorption and scattering (DAS), which is also referred in Tab.1, is the optical interaction where the differential attenuation of two laser beams is evaluated from their backscattered signals when the frequency of one of the beams is closely matched to a given molecular transition while the frequency of the other is somewhat detuned from the transition.

The sensitivity of a laser radar is related to the relative strength of these optical processes through the *lidar equation*. This equation is used to predict the power of the backscattered signal, $P(\lambda,R)$. If an homogeneous atmosphere is assumed, the lidar equation may be given in its simplest form as

$$P(\lambda,R) = \frac{KP_o}{R^2}\beta(\lambda,R)\exp(-2\alpha R) \tag{3}$$

where:

P_o is the transmitted laser power,
K is the optical efficiency of the system,
R is the range to the target,
β is the backscatter-coefficient and,
$exp(-2\alpha R)$ is the two-way atmospheric attenuation of the optical beam.

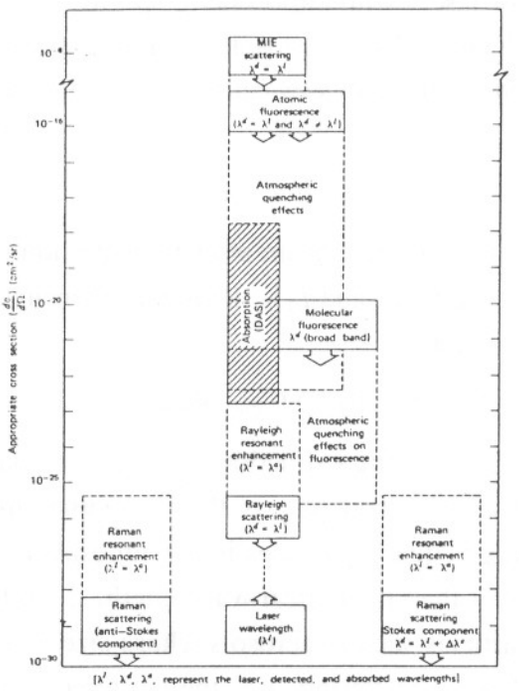

Tab.1 Optical interactions of relevance to laser environmental sensing [25].

A more general form of eq.(3) will be given in Chap.3. The target can be either a solid reflector, such as a building or trees or a semi-infinite reflector consisting of molecules, dust or clouds. In the latter case, the target reflectivity term or backscatter-coefficient, β, is due to Mie, Rayleigh, Raman, or fluorescence processes and is thus also related to the associated α values. *Since all the processes shown in Tab.1 can occur simultaneously, it is important to design the lidar system so that the measurement is most sensitive to only the optical interaction of interest.* (See also Sect.3).

2.3 Laser sources

The availability of lasers with sufficient output power and wavelength characteristics condition an adequate lidar signal. Although many lasers provide high power, they often lack spectral coverage or *tunability*, preventing a determination of the resonant values of the optical parameters, α and β for the particular atmospheric species [33].

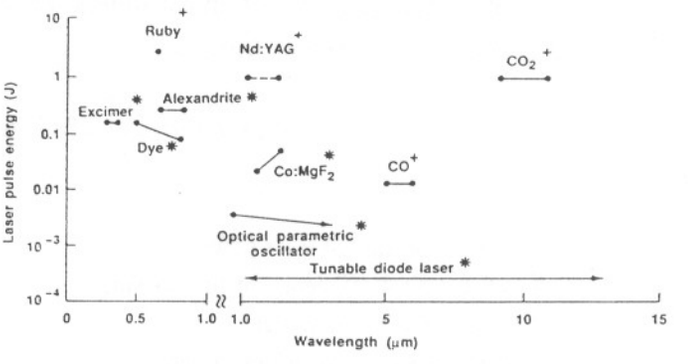

Fig.2 Typical values of laser pulse energy as a function of wavelength tuning range of currently available lasers; (+) line tunable; (*) continuously tunable [22].

On the basis of Fig.2, it is seen that the wavelength tuning range of high-power lasers is not complete across the spectral range shown, being particularly uncovered the *eye-safe* spectral region *($\lambda > 1.4\ \mu m$)*. For remote sensing in the infrared (IR), a minimum laser pulse energy on the order of *1-10 mJ* is required for the detection of lidar signals from a hard target at a range of a few kilometers, and about *1 J* for range-resolved returns from atmospheric aerosols. These values may be lowered by one or two orders of magnitude if heterodyne detection can be used [22].

Historically, most remote sensing experiments have used ruby, dye, neodymium:yttrium-aluminium-garnet (Nd:YAG), and CO_2 lasers. These lasers offer sufficient energy for the detection of atmospheric species at moderate ranges, operate at wavelengths that are not appreciably attenuated by the atmosphere, and occur in a spectral range where several atmospheric constituents have reasonably strong optical interaction. Tab.2 lists relevant lasers to lidar applications (see also [25]).

To carry out the UPC lidar project, a Nd:YAG laser, which is tunable at the fundamental *($\lambda = 1064\ nm$)* and second-harmonic wavelength *($\lambda = 532\ nm$),* has been used.

	Solid State	Gas	Liquid	Semiconductor
Representative examples	Ruby Neodymium (YAG) Alexandrite	XeCl (rare-gas halide) N_2 (transient) $HgBr_2/HgBr$ (dissociation) CO_2 (molecular)	Organic dyes such as: Rhodamine 6G Coumarin Cresyl violet	GaAs GaAsP InAs $Pb_{1-x}Sn_xSe$
Primary pumping technique	Flashlamp	Intense electrical discharge in gas	Flashlamp or laser	High current injection leading to n, p radiative annihilation at an n–p junction
Range of wavelengths and tuning	Ruby (694.3 nm)—thermal tuning ±0.4 nm Nd-YAG (1.06 μm) Alexandrite—tunable (701–818 nm) Second (or third) harmonic generation possible with all three kinds	H_2 (116, 160 nm) Xe_2 (170 nm) KrF (249 nm) XeCl (308 nm) N_2 (337 nm) $HgBr_2/HgBr$ (502–504 nm) DF or HF (2.7–4.0 μm) CO (5.0–5.7 μm) CO_2 (9.0–11 μm) HCN (337 μm)	Large range of dyes provide wavelengths from 340 nm to 1.1 μm Typical tuning range per dye ≈ 40 nm with widths of 0.1–0.01 nm possible with grating or prism (+ etalon) arrangement	GaAsP–$Pb_{1-x}Sn_xSe$ (550 nm to 32 μm) Tuning possible by changing current, applying pressure or magnetic field
Modes of operation and pulse duration	Q-switching leads to 10–100-ns pulses Mode-locking can yield 10-ps pulses	Fast discharges lead to pulses that typically range from 1 ns to 1 μs Q-switching possible with certain molecular gas lasers, cavity dumping with others	When N_2 laser pumped pulses are ~ 5–10-ns When flashlamp pumped 0.3–1-μs pulses Cavity dumping of latter can yield 30-ns pulses	Current pulsed but requires cooling and efficient heat sink 10 ns to 1 μs possible
Peak power and energy/pulse attainable	For ruby and Nd–YAG 10^6–10^8 W and 1–10 J when Q-switched; for Alexandrite lasers 10^7 W and 500 mJ	10^4–10^7 W and 1 mJ to 1 J	10^4–10^6 W in narrow, tunable bandwidth; 0.1–3 J	100 W possible from laser diode arrays

Tab.2 Types of lasers relevant to remote sensing [25].

2.4 Detectors

For wavelengths that lie between *200 nm* and *1 μm* (ultraviolet and near infrared), *photomultipliers tubes (PMTs)* are generally preferred because of their high gain and low noise. Actually, these devices are capable of *single photon counting* [122][128]. Windowless PMTs can be used from the near *UV* through the *X ray* region, and may also be used as particle detectors [136].

The operating principle is quite simple (Fig.3): Photons which strike the PMT's photocathode eject an electron by photoelectric effect. This electron is accelerated towards the first dynode by a potential of *100* to *400 Vdc*. Secondary electrons are ejected when the electron strikes the first dynode, and these electrons are accelerated towards the second dynode. The process continues, typically for *8-14 dynodes,* each providing an electron gain of about *4-5,* to produce 10^6 to 10^7 electrons which are collected by the anode.

PMTs are the quietest detectors available since the primary noise source is thermoionic emission of electrons from the photocathode and from the first few dynodes of the gain chain. PMT housings which cool the PMT to about *-20°C* can dramatically reduce the dark noise. Overall performance of a PMT is determined by these factors:

- *spectral response of the base of the photocathode,*
- *dark-current characteristics,*
- *gain of the dynode chain,*
- *time dispersal effects of the electrons moving through the dynode chain,*
- *rise time, transit time and ringing.*

To continue with, *channel multipliers* are tiny hollow glass tubes with a secondary-emitter coating deposited on the inner walls. When a voltage is applied to such a tube an electron is injected (from a photocathode) and current gains of 10^7 can be achieved [25]. Wafers comprising tens of thousands of such microchannels are commercially available.

Finally, infrared detectors can be divided, broadly speaking, into two classes: *photodetectors and thermal detectors.* The most sensitive infrared detectors are semiconductors in which the incident radiation creates charge carriers via a quantum interaction [153].

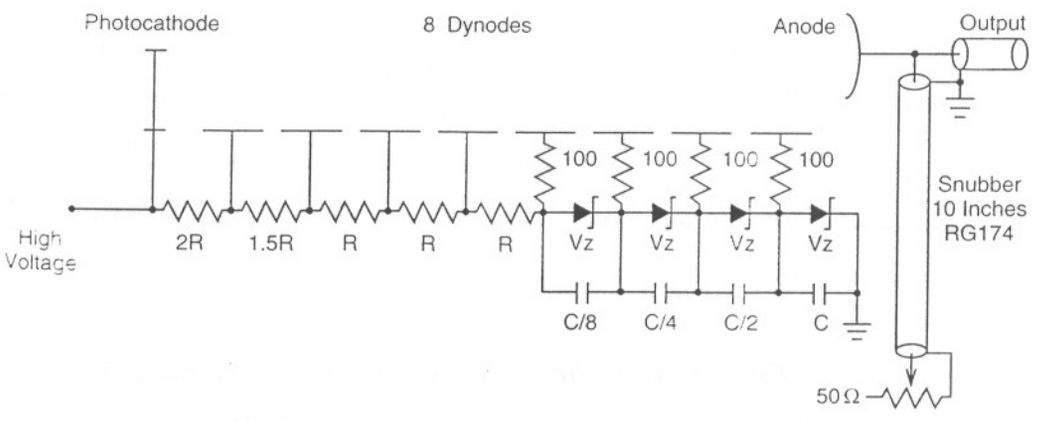

Fig.3 Practical PMT schematic [122].

On top of the photodiodes, there is the *avalanche photodiode or APD*. When operated at a high reverse bias, it develops internal gain though a process of carrier multiplication. APDs are similar to PMTs in that sense that their sensitivity is no longer determined by thermal noise of the detector and output circuit [107][136].

Recently the *Vacuum Avalanche Photodiode*, or *VAPD,* is being introduced into the market. (As far as the author knows, VAPDs from the firms Hamamatsu and DEP have come into the market in 1996). Basically the VAPD mates an APD to a photocathode in a vacuum tube (the APD is treated in more detail in Chap.5).

The working principle can be explained with reference to Fig.4. When photons pass through the glass window, they are absorbed by the photocathode material, which, in response, emits electrons into the vacuum. The electric field accelerates these electrons to the surface of the APD. Upon the impact, electrons from the semiconductor (the internal APD) are promoted into the conduction band. This process is known as Electron Bombardment Induced Conductivity (EBIC). These secondary electrons will experience the second stage of gain in the internal APD, by virtue of the normal avalanche process. The total gain, can be higher that 10^6. Because the photocathode does not contribute much noise, one photon will experience virtually noiseless first stage of gain, which make these devices fairly attractive [136].

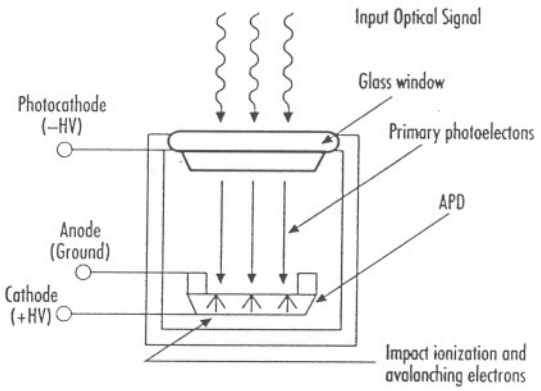

Fig.4 Internal structure of an VAPD [136].

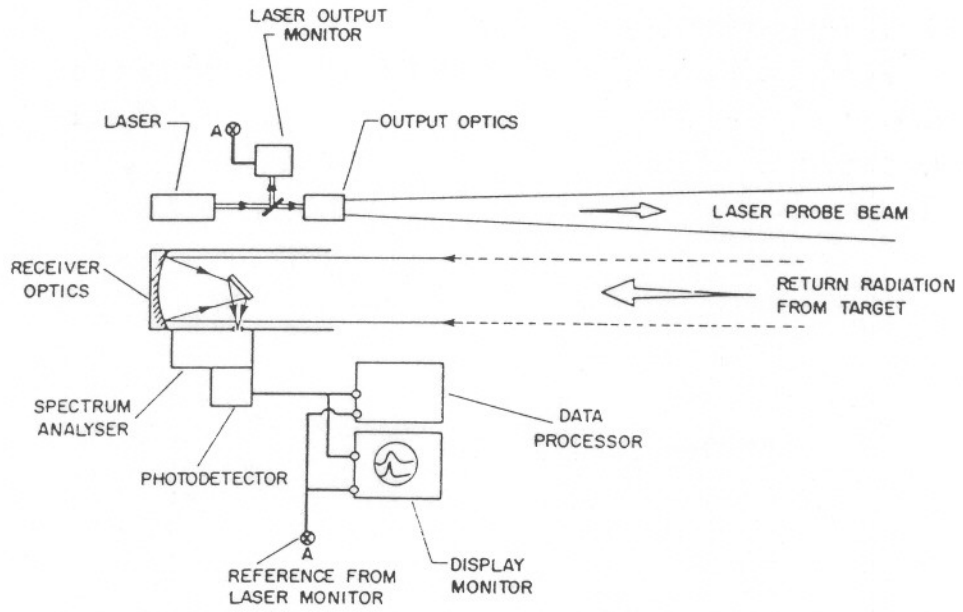

Fig.5 Essential elements of a lidar system [25].

3. REMOTE MONITORING CAPABILITIES OF LIDAR SYSTEMS

This section presents a brief overview of the capabilities of remote-monitoring laser instrumentation. In the atmosphere, remote sensing techniques can be divided into two broad categories: active and passive, depending on the source of radiation. Active techniques, for the purpose of this discussion, will be subdivided into single-ended and double-ended systems, where the principle tecniques for each case are discussed separately, even though, sometimes the subdivision is not very strict.

3.1 Single-ended systems

Single-ended systems, as the name implies, co-locate the laser source and telescope receiver. Fig.5 portrays a biaxial Newtonian system, which is quite similar to the one subject of this thesis except for the telescope configuration.

3.1.1 Elastic-backscatter lidar

Atmospheric backscatter lidar is the most common type of lidar system and it is the case of the one treated in this work (Fig.6). In the most general case, the source is often a nontunable, high-power, Nd:YAG pulsed laser that is used to measure changes in the density or backscatter-coefficient of the atmosphere that are due to particles, such as aerosols, clouds, dust, or plumes. These atmospheric constituents have relatively large

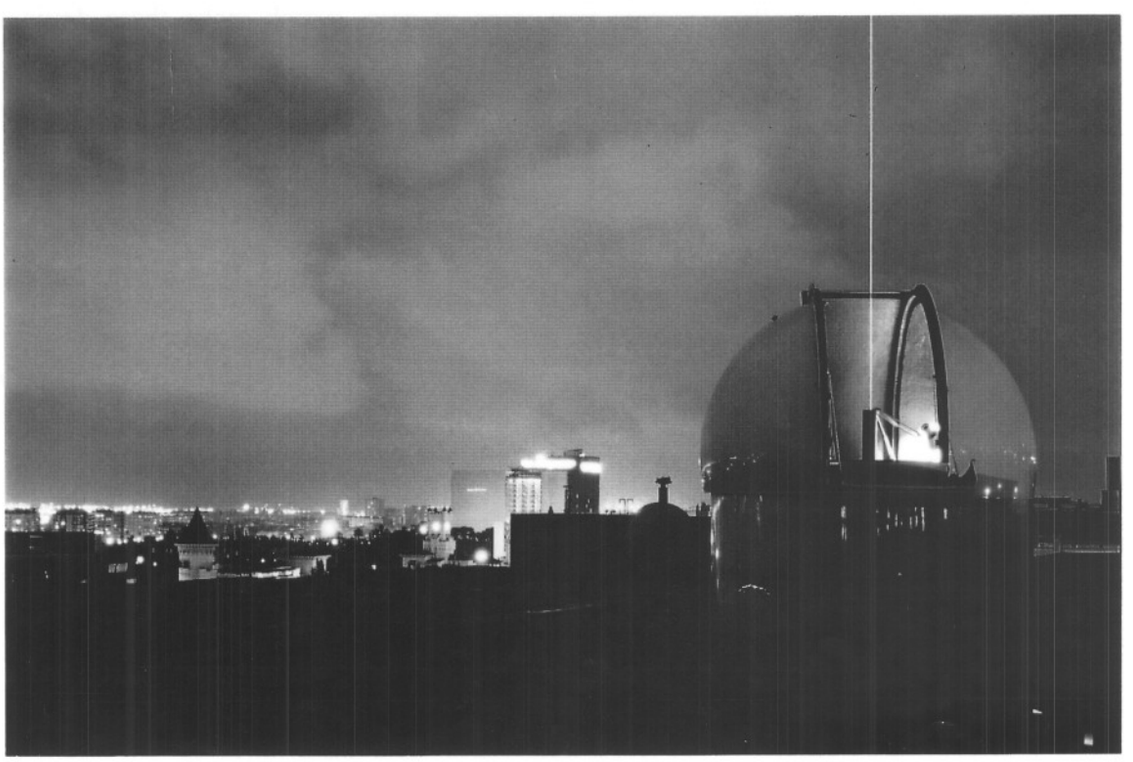

Fig.6 The UPC elastic lidar in operation.

optical scattering cross-sections and are relatively easy to detect. Such lidars have been useful in tracking the turbid effluents and gas plumes from industries chimney-stacks and have also been used to map out rain, snow, ice crystals, and dense clouds in the atmosphere [113]. Precision measurements of the slight changes of the atmosphere have also been made with lidar, from which one can determine the pressure and temperature as a function of altitude [81].

A recent development, based on the principle of Rayleigh scattering, LIMA *(**LI**dar **MA**rine)* is a marine-based system capable of continuously monitoring atmospheric temperature and density at altitudes from *30 to 100 km.* The *Centre National d'Etudes Spatiales (CNES, Paris, France)* uses LIMA for comparing measurements of spacecraft re-entry with their fixed ground stations. The system provides vertical resolution of *150 m,* temporal resolution of *1 min,* and *1 K temperature accuracy* [152].

Wind-speed measurements with a scanning elastic-backscatter lidar have also been made during the 1992 Summer Olympics at Barcelona by *Los Alamos National Laboratory (LANL)* in the Barcelona Air Quality Initiative (BAQI) campaign, which was carried out in collaboration with the meteorological Institute of the UPC (**I**nstitut de **TE**cnologia i **M**odelització **A**mbiental, ITEMA). By correlation of a four-angle scanning pattern, the experiment measured wind speeds around the city [171]. Such data have greatly increased the knowledge of the interplay of air circulation and pollution emission and are being used to predict the impact of contaminant emissions in the urban centre.

The effect of *multiple scattering* has also been investigated by lidar [168][57]; multiple scattering is due to optically thick clouds that can drastically alter the transmission properties of a laser beam from that described by eq.(1) [17].

3.1.2 Differential-absorption lidar (DIAL)

Most lidars that determine the concentration of gaseous species in the atmosphere use DIAL technique [25]. *This technique uses two or more wavelengths to measure the difference in the absorption of the lidar signal as the laser frequency is varied between a wavelength that is absorbed by molecules in the atmosphere and a wavelength that is not absorbed.* The method is sensitive because it takes advantage of the relative large value of the *on-resonance* absorption-coefficient, α.

In principle, the concentration of an atmospheric species may be obtained directly form eqs.(2) and (3) on the basis of measurements at a single wavelength. Yet, a concentration determination based on eq.(3) and a single-wavelength measurement requires an accurate knowledge of K, α, β and R. In general, these parameters are either unknown due to the atmospheric inhomogeneities (α, β) or known with poor accuracy.

The DIAL technique attempts to overcome this problem by measuring the lidar signal at two wavelengths, λ and λ'. The laser wavelength is chosen to coincide with a

wavelength strongly absorbed by the molecule being investigated, while at λ' there is little or no absorption. The use of two wavelengths results in two equations of the form of eq.(3), which are then solved simultaneously for the path-averaged concentration of the absorbing molecule, to yield [22][25]

$$N_a = \frac{1}{2(\sigma_a' - \sigma_a)R}\left[\ln\left(\frac{P_n}{P_n'}\right) + \ln\left(\frac{\beta'}{\beta}\right) + 2(\alpha - \alpha')R\right] \tag{4}$$

where

N_a is the concentration of the absorbing molecule,

σ_a is the absorption cross-section of the absorbing molecule and,

P_n is the backscattered signal power normalized to the transmitted power ($P_n = P/P_0$).

The advantage of the DIAL approach is that only relative differences in the various parameters need be considered. Further simplification can be achieved when the use of closely spaced frequencies results in differences of target reflectivity (backscatter, $\Delta\beta$) and extinction ($\Delta\alpha$) that are negligibly small. In this case eq.(4) reduces to [22][25]

$$N_a = \frac{1}{2(\sigma_a' - \sigma_a)R}\ln\left(\frac{P_n}{P_n'}\right) \tag{5}$$

The lidar systems used in these DIAL measurements span the frequency range from the *UV* to the *IR* and cover both *range resolved* (RR) and path-averaged or *column-content* (CC) measurements.

The molecules investigated in CC DIAL include SO_2, NH_3, O_3, CO, CO_2, HCl, H_2O, NO, N_2H_4, N_2O and SF_6. The sensitivity of many of these CC DIAL measurements is on the order of a few parts per billion to a per parts per million, with detection ranges on the order of several kilometers.

Range-resolved DIAL measurements provide a continuous signal as a function of range and thus, they can provide a three-dimensional mapping of the measured species.

One of the most striking RR DIAL systems was developed by Rothe et al. [29]. They used a *1-mJ, 300-ns, flashlamp-pumped, tunable dye laser* operating between *455* and *470 nm* with a *1-pps* repetition rate to demonstrate that NO_2 concentrations down to *200 ppb* could be detected at night up to a range of *4 km* over the city of Cologne. Their map of NO_2 is reproduced in Fig.7.

Much of the early development work of DIAL systems was done in the UK through a collaboration between *British Petroleum* and the *National Physical Laboratory (NPL, Teddington, UK)*. As an example, DIAL is now offered as a service by the NPL and by *Spectrasyne Ltd.* for monitoring emission of volatile organic compounds. DIAL equipment is contained in a *12-m-long truck* that has been operating across Europe since 1990 and has been involved in many on-site measurements at oil and gas terminals [24].

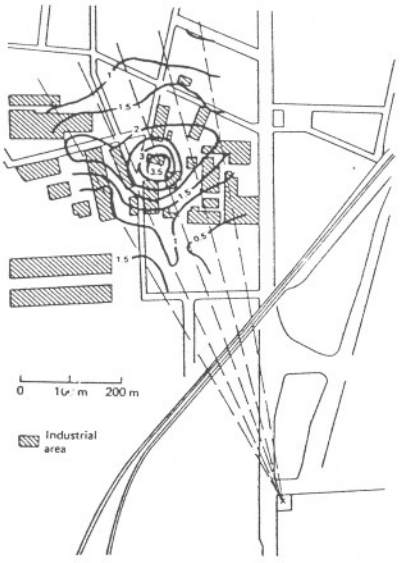

Fig.7 NO_2 distribution over a chemical factory from a DIAL lidar [25].

3.1.3 Fluorescence lidar

In a fluorescence lidar system, the laser is tuned to an absorption line of the species that is to be measured and the reradiated fluorescence is detected by selective spectral filtering of the returned radiation. The fluorescence radiation may be at the same wavelength as the excitation wavelength or may be red-shifted (have a longer wavelength).

Several factors that limit the application of fluorescence lidar for remote sensing include problems involving detector sensitivity coupled with solar background radiation, which generally reduces fluorescence measurements to nighttime and to wavelengths shorter than *1 μm*. In addition, collisions with other molecules before fluorescent emission quench the fluorescent output, rendering it extremely difficult for most remote sensing application in the troposphere or even in the lower stratosphere [9][25]

A significant application of fluorescence lidar involves the study of the hydroxyl free radical, *OH*. Although *OH* occurs as a trace species at very low concentrations (on the order of 0.1 parts per trillion), it plays and important catalytic role in various atmospheric chemistry processes and, together with chlorine and nitrogen oxides, is involved in the O_3 destruction cycle in the atmosphere.

A collaboration between the *Clarendon Laboratory of the University of Oxford (Oxford, UK), Oxford Lasers (Abingdon, UK),* and a German group at *KFA Jülich* aims to develop a *copper-vapor-laser-(CVL)-pumped Ti:sapphire laser* for airborne detection of atmospheric *OH radicals*. High pulse-repetition-rate (2-25 kHz) offers good integration times [24].

In 1983 NASA researchers first demonstrated the technical feasibility of detecting laser-induced chlorophyll fluorescence in plants from low-flying aircraft. In 1990 LASFLEUR EUREKA project was given the final go-ahead. The overall objective was to

detail the biophysical parameters of plants and vegetation canopies that can be deduced from far-field laser-induced temporal and spectral signatures. The chlorophyll fluorescence ratio *F690/F735* (fluorescence at 690 and 735 nm) and blue/red ratio *(F450/F690)* turned out to be two important environmental stress indicators [14].

3.1.4 Raman scattering lidar

The use of Raman scattering methods for remote sensing is severely limited by the *small optical interaction strength for Raman scattering*. As a result, this technique is generally used with high-energy pulsed lasers and is restricted to the UV or visible regions of the spectrum so that sensitive photomultiplier tubes can be used for detection, and is most useful for the detection of species either at close ranges or in high concentration in the atmosphere such as N_2, O_2, and H_2O. It has a range capability of tens of kilometers for the detection of atmospheric N_2 but it is limited to about a few hundred meters for pollution monitoring. In addition, its sensitivity is low (on the order of 100 ppm) as compared with other techniques. Notwithstanding these shortcomings, the most noteworthy feature of Raman scattering is that the laser wavelength does not have to be tuned across an absorption line since the spectral information is given by the frequency shift of the emission, which is independent of the laser wavelength.

The Raman-scattered wavelength-shifted spectra are distinct for each molecular species, which allows separate analysis of the Raman returns from each species. This spectral discrimination can be used to advantage by comparing the relative intensity from atmospheric N_2, whose concentration is known. This ratio approach enables to eliminate instrumental uncertainties in the lidar equation.

A wide variety of Raman lidar measurements of atmospheric pollution species have been made in regions where their concentrations are quite high. In particular, SO_2, NO, CO, H_2S, C_2H_4, CH_4 and H_2CO present in high concentration (100 to 1000 ppm) in oil smoke plumes and automobile exhausts, at ranges on the order of *30* to *100 m [22]*.

Another application of Raman lidar arise from the fact that the backscattered Raman intensity for a given rotational band is strongly temperature dependent. This property has been used for the remote measurement of atmospheric temperature profiles at ranges over *2 km* with an uncertainty of less than ± 2 *K*. [174].

3.1.5 Doppler lidar

Doppler shifts in the return lidar signals have been used to measure wind velocities and to differentiate between molecular and aerosol returns in th atmosphere. Although these shifts are small (a fractional change in frequency of approximately 10^{-8} for a velocity of *1 m/s* at a wavelength of *10* μm), they can be measured by optical heterodyne detection

techniques. Heterodyne detection involves the optical mixing of the lidar return with another laser operation at or near the lidar transmitter wavelength, with detection of the difference of beat frequency of the mixed signal.

This system has yielded information on boundary layer flow near storm gusts fronts and wind shears near airports [133]. Doppler lidar systems have also been used to measure aircraft vortices and clear air turbulence.

Designed and built by SESO *(**S**ociété **E**uropéenne de **S**ystèmes **O**ptiques, [113])* in 1992, the LIMET *(**LI**dar **ME**teorology)* is the first commercial Doppler lidar. It uses a *532-nm* laser that provides *10-ns* pulses at a repetition rate of *10 kHz* with an average power of *1 W* for measuring windspeed and direction at ranges of *30* to *3000 m*. The LIMET provides *1 m/s* accuracy at a height of *500 m* with *150-m* spatial resolution and a *5-min* integration time [152].

3.2 Double-ended systems

Double-ended systems are characterized by either having the laser transmitter and receiver telescope located separately or having the laser and telescope co-located with a physical reflector located at a distance.

3.2.1 Bistatic lidar

In this technique, both the laser and the telescope are aimed towards the same point in the atmosphere. The beam divergence of the laser and the field-of-view of the telescope define the scattering volume at the point of intersection. By carefully varying the pointing angle of both the laser and telescope, measurements of scattering at a fixed altitude can be observed for a variety of scattering angles [9].

3.2.2 Long-path absorption

This technique utilizes the absorption of a laser beam as it propagates through the atmosphere as the measurable parameter to infer molecular concentration. The laser source and telescope receiver can be separated and pointed towards each other; but, for easy operation, the laser and the telescope are generally co-located with their optical axes aligned and pointing to a retro-reflector or topographical target. The system uses differential absorption to interrogate the intervening atmosphere. Comparison of the two signals collected by the telescope provides a measure of the integrated concentration of the molecular species along the transmission path. In some application more than two beams of different wavelength are required because of molecular absorption. A promising outgrowth of this technique is the use of topographical targets as retro-reflectors [9].

4. THE UPC LIDAR SYSTEM

At the Polytechnic University of Catalonia (UPC) at Barcelona, Spain, an elastic-backscatter lidar has been under development (Sect.3.1.1) since 1993.

As discussed in the introduction of this PhD thesis, a main objective of the project was to get acquainted with the lidar technique. To achieve this goal, experiments such as *ceilometry studies (cloud height assessment) and semi-quantitative mapping of aerosol concentrations* were proposed. From the collaboration with the meteorological institute of the UPC, ITEMA, it was agreed that the lidar exploration range should include the boundary layer of the troposphere. Up to this layer, meteorological conditions like water-vapour variations, exert a major influence on aerosol and particle distributions. Remote knowledge of the boundary layer characteristics is quite valuable for the verification and determination of critical input parameters of *urban pollution transport models and weather forecast.* Since typical heights of the boundary layer are between *2-3 km,* the system specification was tightened to reach a minimum height of *5 km* even with moderate visibility margins. (This concept will be defined in Chap.3). Such conservative criterion left room to long range explorations under exceptional visibility conditions.

4.1 Emission configuration

Fig.10 shows the *Nd:YAG Q-switched pulsed laser* by Spectra Physics, model Quanta Ray CGR-130-10 used as light source [118].

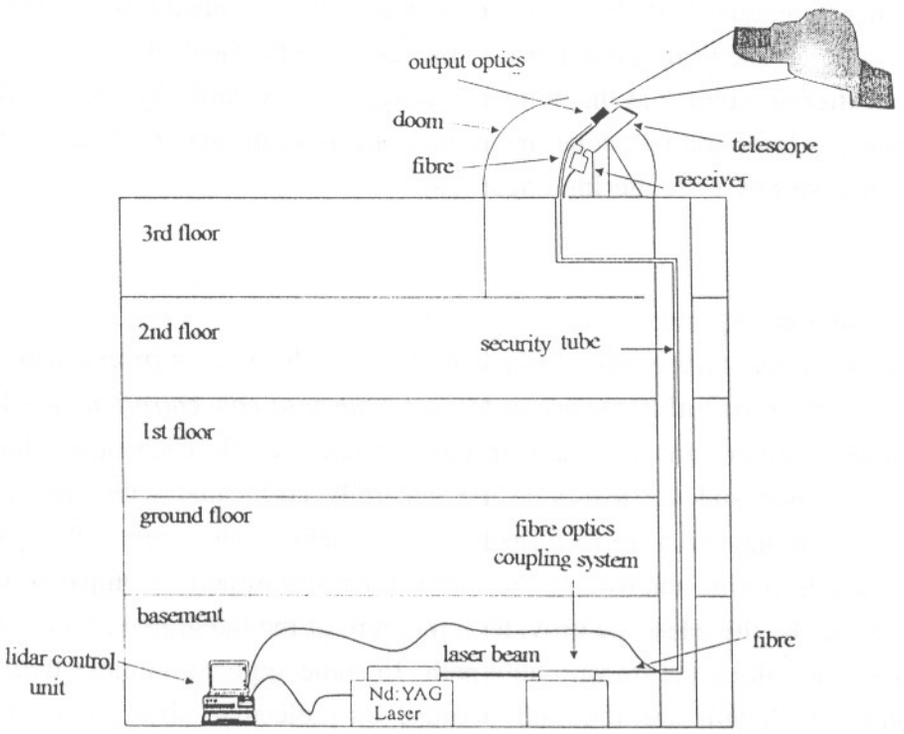

Fig.8 Planned schematic diagram of the UPC lidar system.

The laser produces light pulses with a maximum energy of *1 J* and *10-ns* width at a wavelength of *1064 nm*. With a nonlinear crystal (KDP), these pulses can be transformed to pulses of *500-mJ* energy and *7-ns* duration at the wavelength of *532 nm* [118][116].

As much as the laser's light high emitted energy is of advantage, its size and, therefore, limited manoeuvrability are of disadvantage. To eliminate the need of moving the laser, a guiding system has been designed to carry the light pulses to the emission point. During the design process a system of mirrors as well as a system based on optical fibre were considered. ***This led to two different main configurations to house the whole lidar system:***

The first configuration is to be considered in the short future (about *1997*). Due to the availability and affordability of high-power optical fibres, a layout quite similar to the one shown in Fig.8, where the laser is located in the basement of the building, is planned. For the time being, experimental projects are been carried out with a *TECS39* silica fibre manufactured by *3M, Mod. FT-1.5-UMT,* whose characteristics are:

- *⌀1.5-mm*
- numerical aperture, *NA = 0.39,*
- *10-dB/km* losses and
- a maximum pulsed peak power of *56.6 MW.*

The fibre length is about *30 m* and the same fibre can be used for the two output wavelengths of the laser.

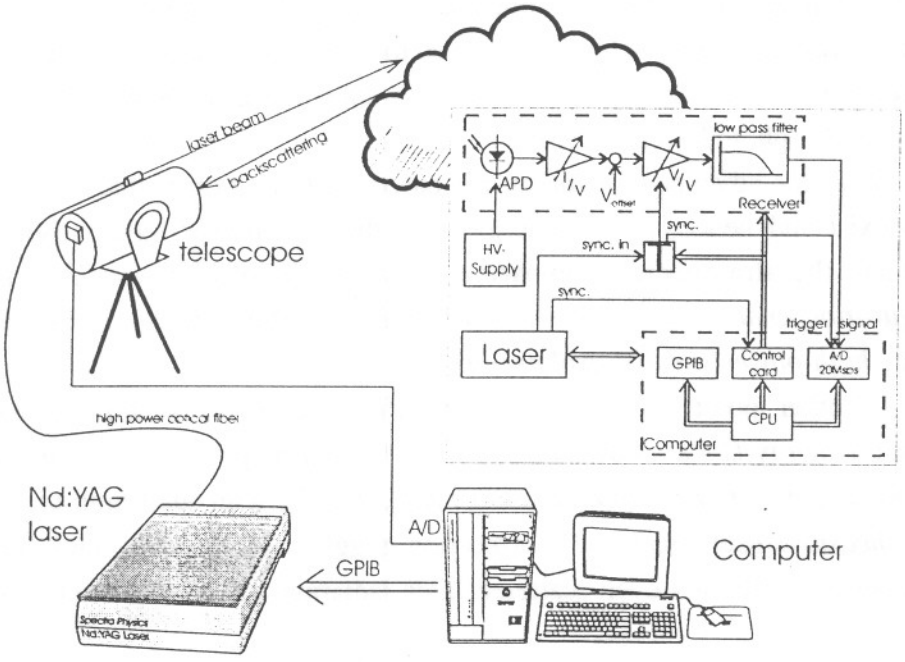

Fig.9 2-D lidar scanner.

Fig.11 shows an experiment conducted with such fibre where the laser output is coupled to the fibre end using high-power lenses and a diaphragm. At the other fibre's end, a green spot is shown projected on the laboratory wall. Despite these encouraging results, some work must still be done to improve the system light throughput, which is hampered by an irregular beam at the laser output giving rise to hot spots when it is focused onto the fiber input end.

In the design of Fig.8, the output optics would consist of two stages. The first one and closest to the laser, would provide efficient coupling and spatial filtering (mode scrambling) while the second one would be mounted on the telescope body to provide as much beam collimation as possible. The set-up of Fig.9, shows the single-ended biaxial arrangement. This solution would enable two-dimensional scans and great flexibility, mainly because the laser beam and the telescope would move together.

As for the second main configuration of the lidar, the laser is located in the control room, which is in third floor of the building, just below the dome (Fig.12). The control room and the dome are communicated by a tube of *10-cm* diameter. The tube houses both the laser beam, which is sent vertically to the atmosphere, in addition to signal and control cables. A plane mirror is enough to guide the optical beam, which leaves the laser output horizontally, to the vertical output.

While output optics is very simple, the alignment of the system warrants some comments. Even though both configurations rely on a biaxial system (that is, the laser beam only enters the field of view of the receiver optics beyond some predetermined range), alignment is further complicated in the mirror-based configuration because the output mirror and the telescope are allowed to move independently. (Biaxial arrangements are preferred in the literature to avoid the problem of near-field backscattered radiation saturating the photodetector [25]).

A prime advantage of the mirror-based configuration is that virtually no coupling losses exist and hence, all the energy from the high-power light pulses is available to illuminate the atmosphere. Comparing the two solutions, *as much as the fibre-based configuration enables low power two-dimensional scans, the mirror-based configuration enables high-power vertical explorations.*

Another point of concern is eye-safety measures. When the laser is fired at maximum energy *(1 J at 1064-nm wavelength),* the peak power is as extremely high as *100 MW.* Since ***Nd:YAG radiation is not eye-safe,*** dealing with such high powers mean ***strict safety measures*** such as class IV protection goggles and interlock-fault alarms. At these power levels direct and even scattered laser radiation can be extremely hazardous to the eye.

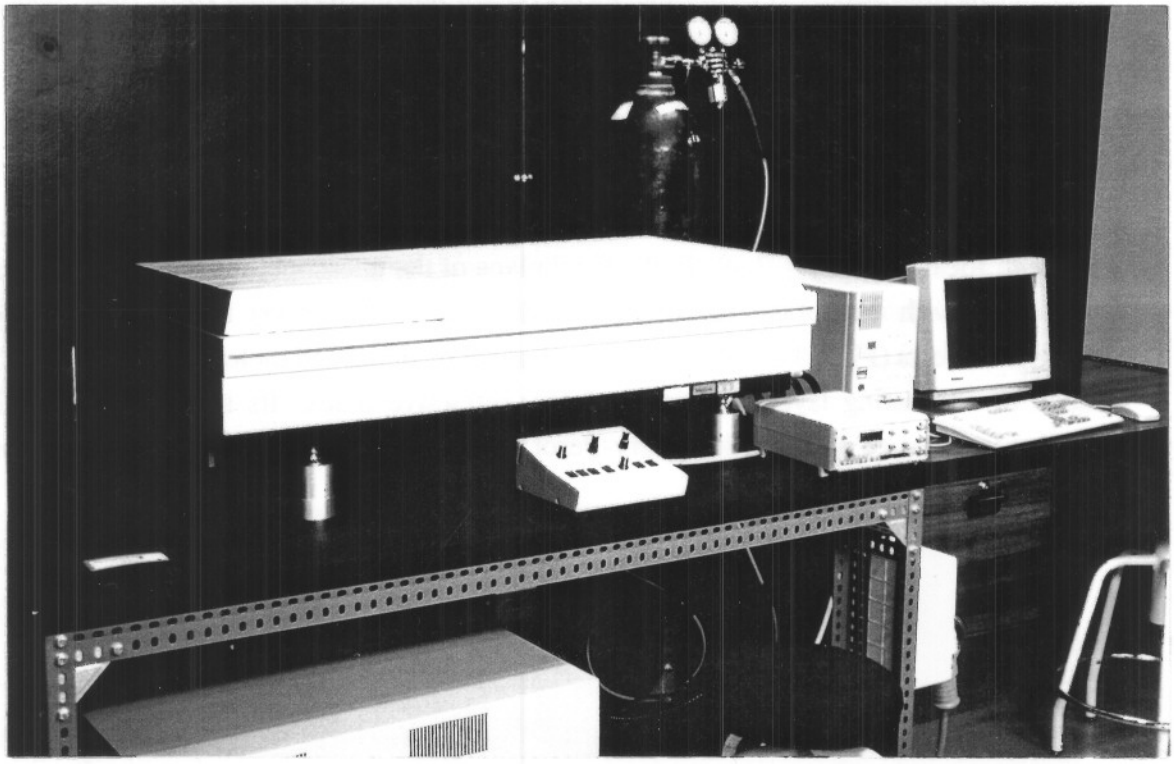

Fig.10 Nd:YAG Q-switched laser (E= 1 J, τ_l< 10 ns, PRF= 10 Hz).

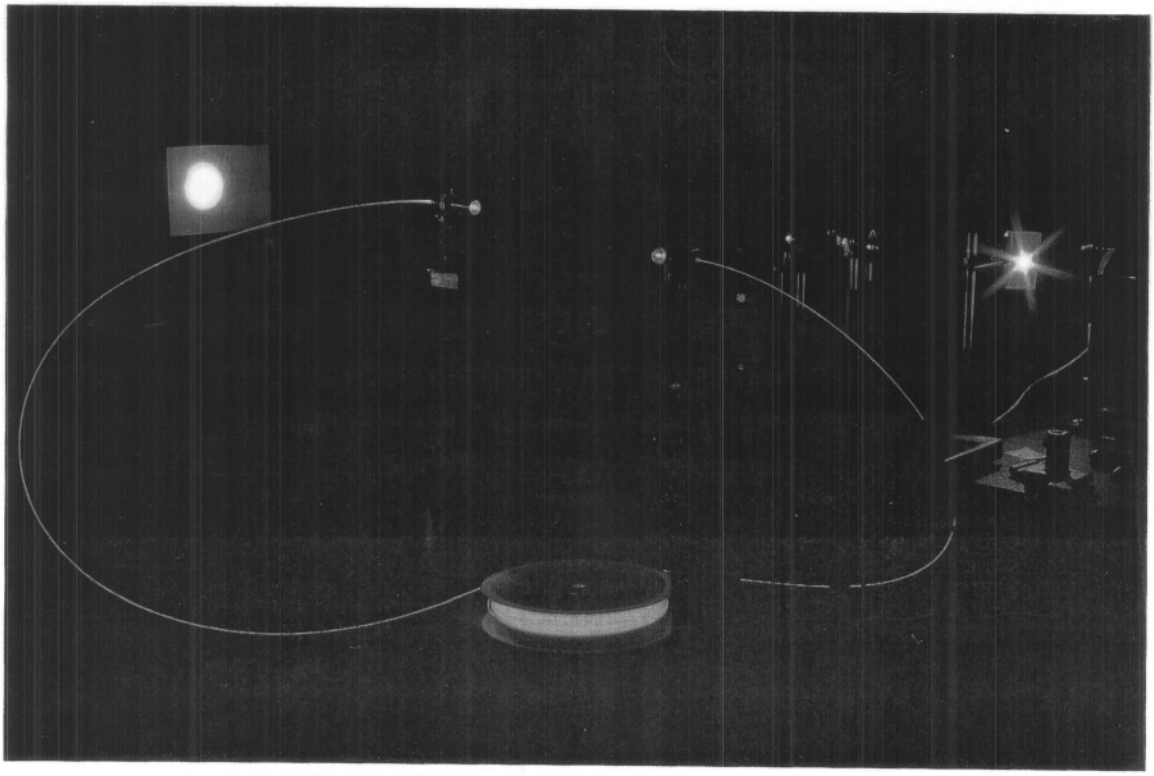

Fig.11 High-power optical fibre experiment.

The lidar activities performed by the author during the period 1993-1996, *which are reported in this PhD thesis, work on the basis of the mirror-based configuration.*

4.2 Receiver systems

The mainstay of the receiver optics is formed by a Cassegranian telescope (aperture *⌀20 cm*, focal length, *f= 2 m*). In the focal plane of the telescope, the receiver is mounted, optionally with an optical narrow band filter *(laser-line filter)* to reduce background radiation effects (Fig.13). The filter is a typical vapor-deposited dielectric interference filter made of alternating layers of high and low refractive index. Its transmission profile is similar to those of a low-order Fabry-Perot interferometer and its bandwidth is *10 nm.*

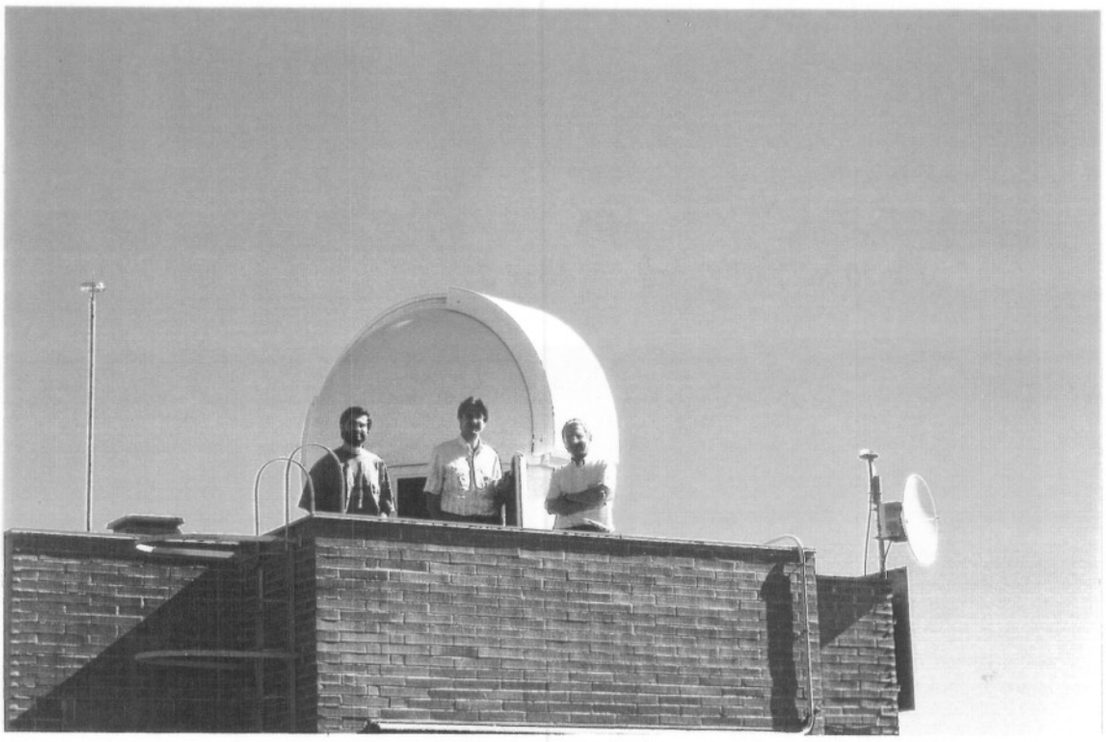

Fig.12 Dome housing the receiver system.

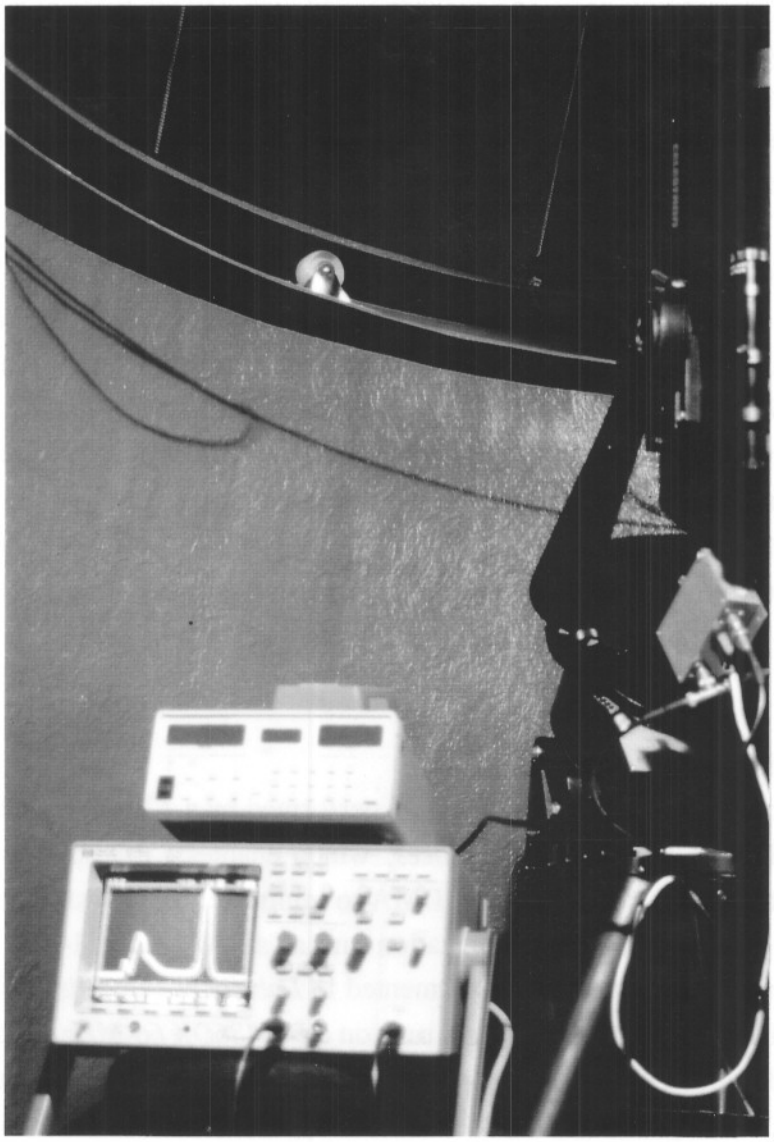

Fig.13 Receiver system into the dome.

The core of the receiver electronics consist of an *APD C30954E avalanche photodiode* from EG&G Optoelectronics and a transimpedance receiver (Fig.14). Based on specifications (see Chap.5 for measurements) the APD has an active area about *0.5* mm^2 and a typical multiplication gain of *120* when biased at *375 V.*

A key feature of this photodetector is the fact that it exhibits similar responsivities at both operating wavelengths *(typ. about 36 A/W at 532 nm and 1064 nm).* Moreover, photodetector gain can be varied by changing the polarization voltage between *15 V* and *400 V.* Thus, at low bias, the photodiode works as if it were a PIN photodiode while at high voltages it works specifically as an APD.

Taking into account expected optical power levels of the return signal (see Chap.3.), versatility, price and ruggedness of such APD in front of typical photomultiplier tubes (PMTs), a decision was made in favour of the above mentioned APD.

The transimpedance receiver (Chap.5) includes two basic amplification stages: a transimpedance amplifier in the first stage to transform the photocurrent of the APD into a voltage, and a conditioning stage (or second stage) formed by a voltage amplifier including an offset correction facility and a low-pass filter with a cut-off frequency of *9.2 MHz*. The receiver front-end incorporates state-of-the-art electronics, such as current feedback operational amplifiers (CFAs), which are suitable for large gain-bandwidth operation. Minimum gain is about *60 dB* and maximum gain is in excess of *100 dB*. System NEP is about *70 fW·Hz*$^{-1/2}$. The conditioning stage fulfils a twofold objective: First, signal conditioning to the input levels of the acquisition system and second, very fast gating control over the receiver (to be explained next, in Sect.4.3).

At the moment, work is under way to develop a new receiver circuit equipped with digital control over gain and offset and adaptive control facilities from the control unit of the lidar.

4.3 Acquisition and control systems

Acquisition of the lidar signal is performed by a *12-bit 20-Msps CompuScope 1012* digitizer from *GaGe Applied Sciences,* which enables *15-m* spatial resolution. The card uses two flash A/D converters and DMA to minimize data transfer times. Data acquisition can be triggered by the synchronization unit as shown in Fig.14.

The control system is implemented in *LabVIEW specialized control software* from National Instruments. The program runs on a *PC 486DX 66-MHz* platform, which includes GPIB and general purpose plug-in acquisition boards to provide interface buses towards the laser, the synchronization unit and the receiver. With them, virtually all lidar parameters can readily be programmed.

Fig.15 shows the control desk during lidar operation. Rather than building a traditional self-contained control unit, with signal input/output capabilities and fixed interface features such as knobs, pushbuttons, graphs and other features, the computer serves as a virtual instrument with open architecture. Thus, the functionality of the interface cards can be user-defined in the control program that can be easily programmed by means of *LabVIEW* graphic language (see Chap.6).

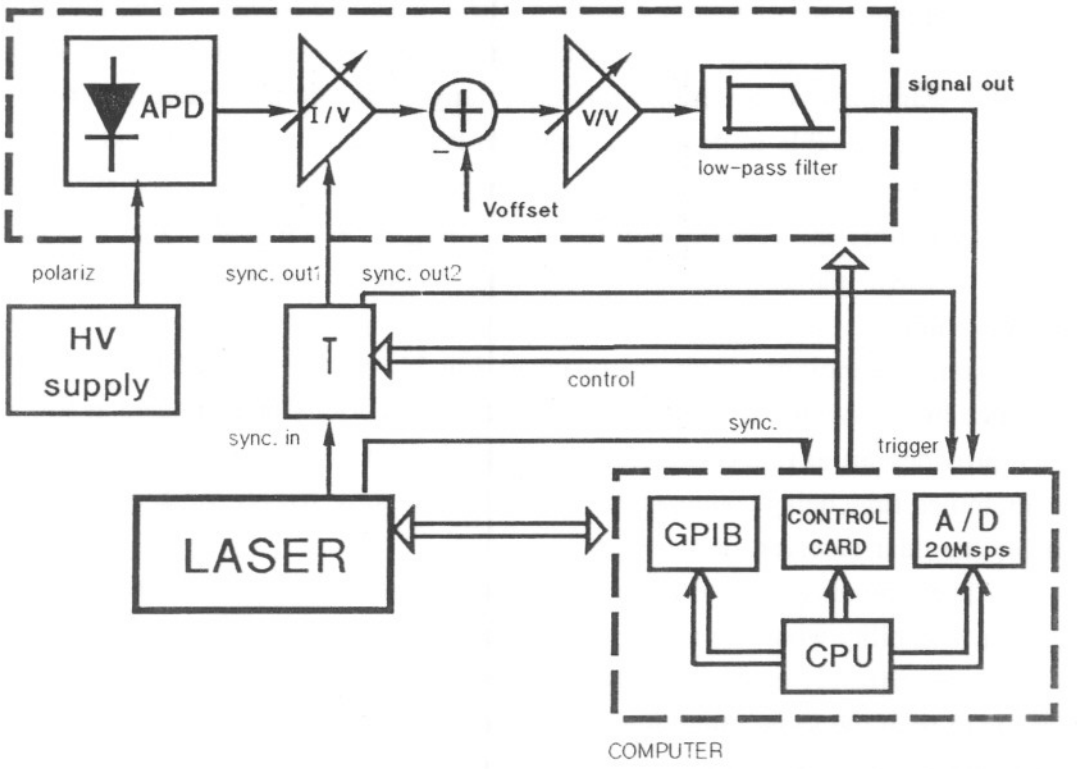

Fig. 14 Reception, acquisition, synchro and control units of the UPC lidar.

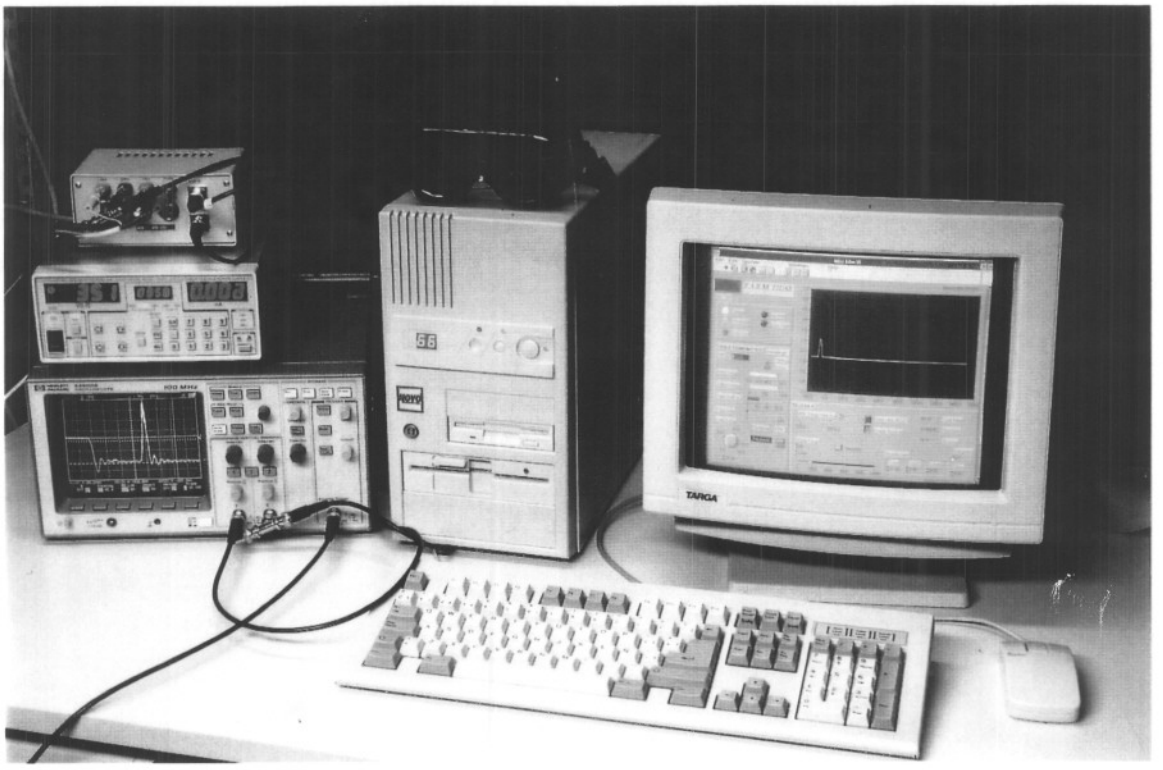

Fig. 15 Lidar system control position.

4.4 Synchronization unit

In applications of remote sensing of the atmosphere where the measurement range is very large (e.g. spanning seven orders of magnitude) it is advisable to provide a feature to enable scanning over different exploration ranges. Should this feature not be available, it would be impossible to deal with exploration ranges between *75 m* and *5 km* or even more. If the minimum exploration range is wished to begin at R_{min}, the synchronization unit must disable the receiver during $\Delta t = 2R_{min}/c$, which is the time needed for the energy to travel the two-way path, and trigger data acquisition in due time, as well. Another function of the synchronization unit is to prevent the acquisition card from unnecessary saturations. With reference to Fig.14, where the synchronization unit is indicated by the symbol *T*, the operating principle can briefly be explained as follows: The laser provides an advanced synchronism signal prior to the pulse output that triggers programmed time delay counts in the unit, which in turn, trigger the acquisition card and enable the lidar receiver.

These points settled, one may well wonder if such unit is not redundant at all, since another possibility would be to trigger the acquisition directly from the laser and leave the receiver permanently enabled. Later, the useless data segment could be discarded. If the lidar is to scan the same range forever, the answer is yes. However, the main advantage arises when scans over different ranges must be interspersed, for instance following a round-robin sequence, and a digital gain programmable receiver is to be controlled by the unit. Under this situation, first the control unit will have to compute the right gain for each scan range and second, it will have to send the computed gain data streams to the synchronization unit. Then, once the gain data streams have been buffered into the synchronization unit, it will have to take over and become responsible for setting the gain parameters of the receiver at the right time. Note that general purpose interface cards of the control unit are not fast enough to do these actions and that in the way explained, the control unit acts, in fact, as a distributed control unit. The synchronization unit will be reviewed in Chap.6.